Surface states of ternary semiconductor alloys: Effect of alloy fluctuations in one-dimensional models with realistic atoms

Garnett W. Bryant
McDonnell Douglas Research Laboratories, P.O. Box 516, St. Louis, Missouri 63166
(Received 30 July 1984)

Calculations of the local electronic surface densities of states (DOS) of semi-infinite one-dimensional chain models for ternary semiconductor alloys are presented to illustrate the effects of alloy fluctuations on semiconductor surface states. The atoms are modeled with a basis set of s and p levels which produces the correct level mixing and energy-band dispersion. Alloys with randomly occupied cation sites are considered. The embedded-cluster approach is employed to incorporate the alloy effects on states localized near the chain end. The cluster calculations are performed by including the contributions from all possible configurations of a cluster at the end of the semi-infinite chain. These results are compared with results obtained using the coherent-potential approximation (CPA) and the virtual-crystal approximation (VCA). The CPA is implemented with one self-energy appropriate for all cation sites in the bulk and different self-energies for each cation site near the surface. In practice the most accurate CPA results can be obtained by treating only the four cation sites nearest the surface differently from the bulk. Examples which are typical of the weak and strong alloy limits are considered. In the first limit the alloy constituents are similar direct-gap semiconductors. In the strong alloy limit one constituent has an inverted band structure, as HgTe does, and the other is a normal semiconductor such as CdTe. The cluster calculation for the surface DOS is sensitive to fluctuations in the environment local to the chain end. In the weak alloy limit, the surface DOS in the band gap has a bimodal distribution with the peaks located near the energies of the surface states of the constituents. In the strong alloy limit, the HgTe-like constituent of the HgCdTe-like alloy has no surface states while the surface states of the CdTe-like constituent lie above the alloy band gap. As a consequence, the alloy surface DOS has a resonance structure above the band edge and band tailing below the edge. The CPA reproduces qualitatively the structure of the cluster calculations. The VCA predicts well-defined surface-state peaks in the band gap. These peaks are related to the average of the bimodal distribution in the weak alloy limit but cannot be consistently identified with any resonance structure or band tailing in the strong alloy limit.

I. INTRODUCTION

In a random substitutional semiconductor alloy either the cation sites, or the anion sites, or both are randomly occupied. The influence of these local fluctuations in occupation on the electronic states of the alloy should depend on the localization of the states in question. States localized to a surface or to a defect should be more sensitive to local alloy fluctuations than bulk states in the valence and conduction bands. As a consequence, the alloy effects should be more dramatic for surface and defect states. To illustrate the effects of alloy fluctuations on the surface states, we have performed a series of calculations using simple semi-infinite one-dimensional chain models to represent ternary semiconductor alloys with randomly occupied cation sites. The alloy effects are incorporated by using the embedded-cluster approximation. In this approach the contributions from all possible configurations of a cluster of sites at the end of the semi-infinite chain are included. The results of these calculations are compared with results obtained using the virtual-crystal approximation (VCA) and the coherent-potential approximation (CPA) to illustrate the capabilities of these effective medium approaches.

This paper reports on calculations done using realistic multistate model atoms for the anions and cations. Basis sets of s and p levels are used to produce semiconductor band structures for the pure constituents which have the correct energy dispersion, the correct admixture of atomic s and p states, and localized surface states in the band gaps. A semi-infinite one-dimensional chain of alternating anion and randomly occupied cation sites is used to model the alloy. The surface is represented by the free end of the chain. A tight-binding Hamiltonian is used to describe the atomic levels and the coupling between nearest-neighbor atoms.

A single state per atom model was used previously[1] by the author to study the effects of alloy fluctuations on surface states and to assess the sensitivity of the effects to the localization of the states. For this simple model, the surface electronic density of states (DOS) tended to separate into DOS appropriate for the individual alloy constituents. This narrowing of the surface bands was also observed in other work on alloy surface states.[2,3] The results also indicated that the more localized the states were to the surface, the more important it was that local fluctuations in site occupation near the surface be incorporated, either in the CPA or the embedded-cluster ap-

proach, to account for the alloy effects.

Although the results of this work are suggestive, the surface states of the pure constituents in the single state per atom model are not localized surface states. Instead they are resonances occurring at the band edges. However, in the multistate model the surface states of the pure constituents are localized to the surface region and their energies do occur in the band gap. Thus the multistate model should better illustrate the alloy effects on semiconductor surface states.

The embedded-cluster approach is no more difficult to implement for realistic model atoms than for the simple model atoms provided that one-dimensional chains are used to model the alloy. In the embedded-cluster approach a finite cluster of sites at the end of the chain is treated exactly and the alloy effects are incorporated by including the contributions from all possible configurations of the cluster. Either the VCA or the CPA is used at the sites not in the cluster to incorporate the bulk alloy effects. By choosing a sufficiently large cluster, the states localized to the surface region are unaffected by alloy fluctuations in the bulk and thus are insensitive to the choice made for the bulk effective medium. By including all alloy configurations of the cluster, a complete description of the alloy effects on states localized near the surface is obtained. The embedded-cluster approach has been used to study the bulk electronic DOS of binary alloys,[4–7] the phonon spectra of one-dimensional model alloys,[8–11] and the alloy broadening at impurity levels in one-dimensional binary alloys.[12,13]

The CPA for realistic atoms can be implemented just as it was implemented for the simple model Hamiltonians.[1] In the CPA the alloy is modeled by an effective medium in which a complex self-energy is assigned to each randomly occupied site. The self-energy at a given site is adjusted self-consistently to reproduce the average scattering at that site due to the possible occupations at that site.[14,15] In the bulk of a ternary semiconductor alloy all of the randomly occupied sites are equivalent so the same self-energy can be used for each randomly occupied bulk site. The CPA has been successfully applied to the study of bulk states in many ternary semiconductor alloys.[16–20]

A surface or defect breaks the translational symmetry and the self-energy becomes a function of position relative to the surface or defect. As a consequence, near a surface a self-consistent self-energy must be found for each plane of equivalent sites. Moreover, the self-energy for a given plane depends on the self-energies of the other planes, because these other self-energies determine the carrier propagation through the alloy. Berk[2] was the first to apply the CPA to the study of the surface states of a cleaved alloy surface. He tested several methods of decoupling the equations used to determine the self-energies of sites in different planes parallel to the surface. Berk found that the self-energy for the surface plane differed from the bulk self-energy, but that the self-energies for other planes were nearly identical to the bulk self-energy. This healing of the self-energy after one plane motivated his surface-bulk approximation. In this approach the bulk self-energy was used for sites in all planes except for the surface and a different self-energy was used for the surface. Others[21,22] have also used the surface-bulk approximation introduced by Berk. In addition the CPA has been used[23,24] to study a randomly occupied monolayer on an ordered substrate. In this case only the surface self-energy need be found. Although the VCA has been used to study realistic semiconductor alloy surface states,[25–31] no use of the CPA has been made for this purpose.

Alloy effects should be stronger for surface states in one-dimensional chains and for adsorbate and defect levels than for three-dimensional surface states because the DOS of localized states is sensitive to the number of sites sampled by the states. Two conditions determine the number of sites sampled by a state: the localization of the state and the coordination number of the lattice. For example, surface states in three-dimensional systems are extended parallel to the surface and can average over fluctuations in occupation in these directions. Surface states in one-dimensional chains and adsorbate and defect levels are localized in every direction and average over fewer sites. In addition, the coordination number is larger in three-dimensional systems, providing more sites for sampling in these systems. The self-energy should heal slowly in systems where the states sample few sites. In fact, the healing occurred after three layers for our previous one-dimensional calculations[1] rather than after the first layer as found by Berk for three-dimensional models.

The slower healing expected for the cases we consider is incorporated by using the natural extension of Berk's surface-bulk approximation. A multisurface approximation in which the self-energy is allowed to differ from the bulk self-energy for as many sites away from the surface as is necessary to account for the slower healing has been employed.

In Sec. II a description of the calculations is given. First, the model Hamiltonian is introduced. The Green's-function formalism is employed to implement the CPA and to determine the bulk and surface DOS. A real-space renormalization procedure is used to evaluate the Green's function. This procedure is described in detail. The results found using the VCA, the CPA, and the embedded-cluster approach are presented and compared in Sec. III. Two examples are discussed. In the first one, the alloy constituents have the direct-gap semiconductor band structure with nearly identical gaps so that the alloy effects should be small. In the other example one constituent is like HgTe with an inverted band structure and the other is like CdTe with a normal band structure. The alloy effects on surface states are more severe in this case. Conclusions are presented in Sec. IV.

II. THEORY

A. The model

The model Hamiltonian used in our calculations is a nearest-neighbor tight-binding Hamiltonian analogous to the sp^3s^* model of Vogl, Hjalmarson, and Dow.[32,33] The Hamiltonian is used to model both semiconductors with finite-energy band gaps, such as GaAs and CdTe, and zero-gap semiconductors, such as HgTe. Specifically, in our model each atom has an s state and two p states. The

cation: p + s
anion: p

heavy-hole and light-hole valence bands of the normal semiconductor band structure are derived from the two anion p levels and the lowest conduction band is derived from the cation s level. For the zero-gap semiconductor, this light-hole band has positive effective mass and becomes the lowest conduction band in the inverted band structure. In addition to these states, the anion also has an excited s level. The s^* state is included so that the normal semiconductor (i.e., CdTe) and the zero-gap semiconductor (HgTe) have direct gaps in our model. One could also consider indirect-gap semiconductors. In this study we restrict our attention to direct-gap semiconductors and refer to those with a finite direct gap as "normal." The anion p state responsible for the split-off valence band, the analogous cation p state, and the s^* cation state are ignored since they do not qualitatively affect the upper valence bands and the lowest conduction band. The atomic levels and the bands of normal- and zero-gap semiconductors that result from these levels are shown schematically in Fig. 1.

With this basis the Hamiltonian matrix for an infinite chain has the block-tridiagonal form,

$$\overline{H}=\begin{pmatrix} \ddots & & & & \\ & H_c & T_{ca} & & 0 \\ & T_{ca}^{+} & H_a & T_{ac} & \\ & & T_{ac}^{+} & H_c & T_{ca} \\ 0 & & & T_{ca}^{+} & H_a \\ & & & & \ddots \end{pmatrix}. \tag{1}$$

The 3×3 diagonal submatrix H_c and the 4×4 diagonal submatrix H_a are the Hamiltonians for the constituent cation and anion, respectively:

$$H_c=\begin{pmatrix} E_{p_c} & 0 & 0 \\ 0 & E_{p_c} & 0 \\ 0 & 0 & E_{s_c} \end{pmatrix}, \tag{2}$$

$$H_a=\begin{pmatrix} E_{p_a} & 0 & 0 & 0 \\ 0 & E_{p_a} & 0 & 0 \\ 0 & 0 & E_{s_a} & 0 \\ 0 & 0 & 0 & E_{s_a^*} \end{pmatrix}.$$

The labeling of the atomic energy levels indicates the order of the basis states in Eqs. (1)–(2). In a real compound semiconductor the light-hole and heavy-hole p valence states are derived from the anion p states with total angular momentum $j=\frac{3}{2}$. The p states in our model are analogous to these states and are ordered with $j_z=\frac{3}{2}$ and $\frac{1}{2}$, respectively, provided that the chain direction is treated similarly to the X direction in a crystal.

The off-diagonal matrices T_{ca} and T_{ac} and their respective adjoints provide the coupling between states on adjacent atoms,

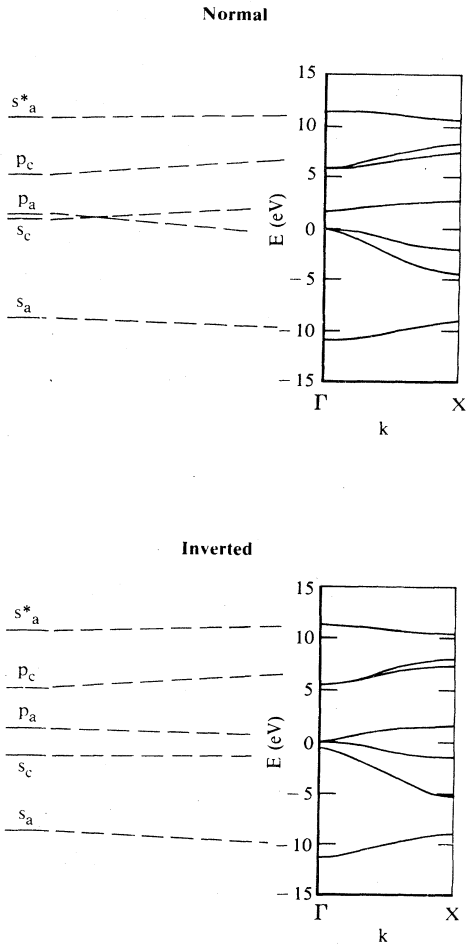

FIG. 1. Normal and inverted band structure. The atomic energy levels responsible for the bands are indicated on the left-hand side. The anion (a) and cation (c) s and doubly degenerate p levels are shown. The band structures were obtained using the parameters in Table I. $E_{s_c}=0.65$ eV for the normal structure and $E_{s_c}=-1.6$ eV for the inverted structure.

$$T_{ca}=\begin{pmatrix} P_1 & iP_2 & 0 & 0 \\ -iP_2 & P_1 & 0 & 0 \\ S_1 & 0 & S_2 & S^* \end{pmatrix}, \tag{3a}$$

$$T_{ac}=\begin{pmatrix} P_1 & -iP_2 & -S_1 \\ iP_2 & P_1 & 0 \\ 0 & 0 & S_2 \\ 0 & 0 & S^* \end{pmatrix}. \tag{3b}$$

The coupling, P_1, between p states on adjacent atoms with the same j_z is different from the coupling, P_2, between p states with different j_z. Moreover, the cation s state couples (S_1) to the anion $p_{3/2}$ state but not to the anion $p_{1/2}$ state. As a result, the band derived from the $p_{3/2}$ state is more strongly repelled by the cation s band and becomes the light-hole band. The band derived from the anion

$p_{1/2}$ state is flatter and is the heavy-hole band. No other couplings to p states are needed to obtain qualitatively correct band structures. The cation s state couples to both anion s states as well as to the anion $p_{3/2}$ state. As mentioned before, the coupling, S^*, of the cation s state to the s^* anion state is needed to insure that the band gaps occur at Γ.

The alloy disorder is assumed to arise from randomly occupied cation sites. Thus the results are relevant to alloys such as $In_{1-x}Ga_xAs$ and $Hg_{1-x}Cd_xTe$. Furthermore, only diagonal disorder is considered and, in particular, only the cation s level is different for the two cations. The assumption of only s state disorder was made to simplify the calculations. However, the assumption is a reasonable first approximation for many semiconductor alloys because the largest differences in energy levels often occur for the s states.[32] The assumption of no off-diagonal disorder was also made to simplify the calculations. However, for realistic systems, one often has sufficient freedom in choosing the tight-binding parameters that the differences in the off-diagonal matrix elements of the alloy constituents can be minimized.[18–20]

For an alloy of the form $C_{1_{1-x}}C_{2_x}A$ the s orbital energies at the cation are E_{s_1} and E_{s_2} with probabilities $1-x$ and x, respectively. Both the VCA and the CPA replace the true Hamiltonian [Eqs. (1)–(3)] with an effective medium to describe the alloy. In the VCA the random cation s level is replaced by the average value

$$E_{s_{\mathrm{VCA}}}=(1-x)E_{s_1}+xE_{s_2}\ . \tag{4}$$

In the CPA the cation s level energy at site i is replaced by a self-energy $\Sigma_i(\omega)$ which depends on the site i and energy ω. In the bulk all cation sites are equivalent and the self-energy is independent of site. However, Σ is site dependent near a surface or a defect.

B. The Green's function and the renormalization approach

Using the Green's function,

$$G(\omega)=(\omega-\bar{H})^{-1}\ , \tag{5}$$

the density of states of level n_i at site i is

$$\rho_{n_i}(\omega)=-\frac{1}{\pi}\,\mathrm{Im}[G_{n_in_i}(\omega)]\ , \tag{6}$$

provided that ω has a small, positive, imaginary part.

A renormalization approach[34–36] has been used to evaluate the Green's function. In this approach alternate sites on the chain are eliminated and the equations for the Green's function are used to define a new effective Hamiltonian with renormalized diagonal elements for the remaining sites and renormalized interactions between the remaining adjacent sites. This decimation procedure is repeated until the separation between remaining adjacent sites is so large that the effective interaction is unimportant. In that limit, the site diagonal Green's function for a site i is the inverse of $\omega-H_i$, where H_i is the effective Hamiltonian for site i.

Alloy effects can be included approximately using the renormalization approach[35,36] by averaging the renormalized matrix elements to account for the alloy effects of the eliminated atoms. However, in this paper the renormalization approach is used only as a calculational tool employed to reduce the effort needed to evaluate the Green's function. The alloy effects are incorporated by using either the VCA or the CPA as an effective medium or by implementing the embedded-cluster approach.

For a semi-infinite chain of atoms with the surface site at site 1 and the Hamiltonian written in block-tridiagonal form,

$$\bar{H}=\begin{bmatrix} H_1 & T_{12} & & & \\ T_{21} & H_2 & T_{23} & & 0 \\ & T_{32} & H_3 & T_{34} & \\ & & T_{43} & H_4 & \\ 0 & & & & \ddots \end{bmatrix}\ , \tag{7}$$

the equations for the Green's function are ($\bar{1}$ is the unit matrix and G_{ij} is the submatrix of the Green's function which connects sites i and j),

$$\begin{aligned}
&(\omega-H_1)G_{11}-T_{12}G_{21}=\bar{1}\ ,\\
&-T_{21}G_{11}+(\omega-H_2)G_{21}-T_{23}G_{31}=0\ ,\\
&(\omega-H_1)G_{13}-T_{12}G_{23}=0\ ,\\
&-T_{21}G_{13}+(\omega-H_2)G_{23}-T_{23}G_{33}=0\ ,\\
&-T_{32}G_{23}+(\omega-H_3)G_{33}-T_{34}G_{43}=\bar{1}\ ,\\
&-T_{43}G_{33}+(\omega-H_4)G_{43}-T_{45}G_{53}=0\ ,\\
&\vdots
\end{aligned} \tag{8}$$

When the first two equations are solved to eliminate site 2, the new renormalized equation is

$$[\omega-H_1-T_{12}(\omega-H_2)^{-1}T_{21}]G_{11}-T_{12}(\omega-H_2)^{-1}T_{23}G_{31}=\bar{1}\ . \tag{9a}$$

Site 2 can be eliminated from the next two equations yielding,

$$[\omega-H_1-T_{12}(\omega-H_2)^{-1}T_{21}]G_{13}-T_{12}(\omega-H_2)^{-1}T_{23}G_{33}=0\ . \tag{9b}$$

Sites 2 and 4 can be eliminated from the last three equations to obtain

$$-T_{32}(\omega-H_2)^{-1}T_{21}G_{13}+[\omega-H_3-T_{32}(\omega-H_2)^{-1}T_{23}-T_{34}(\omega-H_4)^{-1}T_{43}]G_{33}-T_{34}(\omega-H_4)^{-1}T_{45}G_{53}=0\ . \tag{9c}$$

Other equations for the decimated chain are derived similarly. By inspection, the renormalized Hamiltonian $\tilde{H}$ is given by the block matrices:

$$\tilde{H}_1 = H_1 - T_{12}(\omega - H_2)^{-1}T_{21} , \tag{10a}$$

$$\tilde{H}_3 = H_3 - T_{32}(\omega - H_2)^{-1}T_{23} - T_{34}(\omega - H_4)^{-1}T_{43} , \tag{10b}$$

$$\tilde{T}_{13} = T_{12}(\omega - H_2)^{-1}T_{23} , \tag{10c}$$

$$\tilde{T}_{31} = T_{32}(\omega - H_2)^{-1}T_{21} , \tag{10d}$$

$$\vdots$$

where the even sites have been eliminated. Equations (10a) and (10b) are different because the site at the chain end interacts with only one neighbor. Also,

$$\tilde{T}_{31}(\omega)^{+} = \tilde{T}_{13}(\omega^{*}) .$$

If all of the sites to be eliminated in a decimation step are equivalent and all of the bulk sites to remain are equivalent, i.e.,

$$H_2 = H_4 = H_6 = \cdots ,$$

$$H_3 = H_5 = H_7 = \cdots ,$$

$$T_{12} = T_{34} = T_{56} = \cdots ,$$

$$T_{23} = T_{45} = T_{67} = \cdots ,$$

then the same renormalization can be applied to all bulk sites and all of the remaining bulk sites will be equivalent after the decimation. Thus, for the surface site

$$\tilde{H}_1 = H_1 - T_{12}(\omega - H_2)^{-1}T_{21} \tag{11a}$$

and for all bulk sites

$$\tilde{H}_{\text{bulk}} = \tilde{H}_3 = H_3 - T_{12}(\omega - H_2)^{-1}T_{21} - T_{32}(\omega - H_2)^{-1}T_{23} . \tag{11b}$$

The coupling between sites is

$$\tilde{T}_{13} = \tilde{T}_{35} = \cdots = T_{12}(\omega - H_2)^{-1}T_{23} , \tag{11c}$$

and similarly

$$\tilde{T}_{31} = \tilde{T}_{53} = \cdots = T_{32}(\omega - H_2)^{-1}T_{21} . \tag{11d}$$

To study cation terminated chains, the renormalization procedure is first applied to eliminate all anions, leaving a chain of cations with effective cation-cation interactions. This renormalization procedure is then applied repeatedly to the effective cation chain until so many sites have been removed that the effective interaction between remaining sites is negligible. Then the site-diagonal Green's function at the surface cation is obtained by inverting $\omega - \tilde{H}_1$ and the bulk cation site-diagonal Green's function is obtained by inverting $\omega - \tilde{H}_{\text{bulk}}$. One benefit of eliminating the anions and working with effective cation chains is that all additional renormalizations require inversions of matrices that are only 3×3.

When N decimations are performed, $2^N - 1$ sites are removed between remaining sites. Typically we perform 18 decimations of the effective cation chain. In this case 262 143 cations are removed between remaining sites. This number is sufficient to guarantee convergence of the procedure in the cases considered.

To consider a chain terminated by an anion or to consider a chain terminated by a cluster of atoms which are treated differently from the bulk, one must be able to add additional atoms to a cation terminated chain. Consider the effect of adding another atom to the chain defined by the Hamiltonian of Eq. (7). The new Hamiltonian is

$$\bar{H}' = \begin{pmatrix} H_0 & T_{01} & & \\ T_{10} & H_1 & T_{12} & 0 \\ & T_{21} & H_2 & \\ 0 & & & \ddots \end{pmatrix} . \tag{12}$$

The Green's function G' for the new chain is found using the Green's function for the old chain. The site-diagonal Green's function for the new surface atom at site 0 is

$$G'_{00} = (\omega - H_0 - T_{01}G_{11}T_{10})^{-1} \tag{13}$$

and the site-diagonal Green's function at site 1 becomes

$$G'_{11} = (G_{11}^{-1} - T_{10}(\omega - H_0)^{-1}T_{01})^{-1} . \tag{14}$$

Using this prescription, extra atoms can be added iteratively to the chain.

C. Implementation of the embedded-cluster approach

To implement the embedded-cluster approach the renormalization method is first used to determine the Green's function for a semi-infinite chain. The VCA or CPA is used to describe the alloy effects of the chain. Then a cluster of atoms is added to the end of the chain using the iterative procedure discussed in the preceding section. Each added atom is treated exactly by using the original unrenormalized site Hamiltonian [Eqs. (2)—(3)] to describe the atom. The DOS are obtained by including the contributions for all possible cluster configurations. Site occupation is assumed to be random for each cation site.

D. Implementation of the CPA

To implement the multisurface CPA in which the self-energies for the cation s levels at sites near the surface are different from the bulk self-energy, the renormalization approach is first used to determine the Green's function for a semi-infinite chain using the bulk self-energy for each cation s level. Then a cluster of atoms is added to the chain. Each cation in the cluster is described using a self-energy for the s level different from the bulk self-energy.

The CPA for the bulk cation sites is implemented by adjusting the bulk self-energy for a cation s level, Σ_b, until Σ_b produces the same multiple scattering of an electron

bulk is found through procedure above

with energy ω at a bulk cation site as is due to alloy fluctuations in the s level at that site. The t matrix for scattering from the s level at a bulk cation site that is occupied by cation i and embedded in the effective medium is

SAKURAI, 6.1.31

$$t_i = \frac{E_{s_i} - \Sigma_b(\omega)}{1 - [E_{s_i} - \Sigma_b(\omega)] G^b(\omega, \Sigma_b)} , \quad (15)$$

where $G^b(\omega, \Sigma_b)$ is the diagonal Green's function for a bulk cation s level in an alloy described by the CPA effective medium. The t matrix is a scalar because only one level undergoes alloy fluctuations.

In principle, Σ_b is adjusted so that the average scattering due to alloy fluctuations at a site embedded in the effective medium vanishes:

$$(1-x)t_1 + xt_2 = 0 . \quad (16)$$

The self-consistent determination of Σ_b is usually done by iterating Eqs. (15) and (16), starting with an initial guess for Σ_b. However, there is no guarantee that the standard iterative procedures will be stable or converge to the correct solution.[37]

In practice we use the iterative average t-matrix approximation scheme (IATA) of Chen[37] to obtain the CPA self-energies. In the ATA an effective medium, $\Sigma_j(\omega)$, for the s level at each cation site j is defined. Then the multiple scattering from the s level at site j due to a cation of type i at the site j is

$$t_i^j = \frac{E_{s_i} - \Sigma_j(\omega)}{1 - [E_{s_i} - \Sigma_j(\omega)] G^j(\omega, \{\Sigma_k(\omega)\})} \quad (17)$$

where $G^j(\omega, \{\Sigma_k(\omega)\})$ is the diagonal Green's function of the s level at site j for an electron moving in the effective medium defined by the $\{\Sigma_k(\omega)\}$. If $\langle t^j \rangle$ denotes the alloy averaged t matrix,

$$\langle t^j \rangle = t_1^j(1-x) + t_2^j x ,$$

then the ATA for the new self-energy at site j, $\tilde{\Sigma}_j$, that describes the old effective medium Σ_j plus the effect of alloy fluctuations not included in Σ_j is[37]

ti comes from (15)

$$\tilde{\Sigma}_j(\omega) = \Sigma_j(\omega) + \langle t^j \rangle / [1 + \langle t^j \rangle G^j(\omega, \{\Sigma_k(\omega)\})] . \quad (18)$$

Obviously, if Eq. (18) can be iterated to self-consistency so that $\tilde{\Sigma}_j = \Sigma_j$, then $\langle t^j \rangle = 0$ and Σ_j is the CPA self-energy. As Chen has shown and our experience confirms, iteration of Eq. (18) leads to the CPA self-energies. The convergence is rapid except near band edges, but even there the iteration always converges to the CPA solution.

no net transfer

self-consistency

The CPA is implemented by first finding Σ_b, assuming that Σ_b is the same for each bulk site. With use of Σ_b for the bulk, the site-dependent Σ_i near the surface are then found using Eq. (18). The set of equations for the Σ_i in the surface region is iterated simultaneously even though each G^j depends on all $\{\Sigma_k\}$. No trouble was encountered obtaining self-consistent solutions in the surface region. With use of Σ_b as an initial guess for the Σ_i, the convergence for the Σ_i in the surface region is often faster than for Σ_b. Surface regions with up to eight cations treated differently from the bulk were considered. There was no indication that any difficulty would arise if the surface region included more sites.

III. RESULTS

The effects of alloy fluctuations on surface states are presented for two model alloys. One alloy is a mixture of two similar normal compound semiconductors, as in $In_{1-x}Ga_xAs$, while the other is a mixture of two dissimilar compound semiconductors, as in $Hg_{1-x}Cd_xTe$. The first choice illustrates the limit when the alloy effects should be small and the second, when the alloy effects should be large. The parameters used to describe the band structure of the constituent compound semiconductors are listed in Table I. The same value of each parameter except E_{s_c} is used for each constituent. Thus all alloy effects arise from variations in E_{s_c}. By varying E_{s_c} between -1.8 and 0.65 eV, one can obtain compounds with band structures ranging from the inverted structure of HgTe to the normal structure of CdTe with a band gap of 1.558 eV. This parametrization was modified from the one used by Hass *et al.*[20] to model HgTe and CdTe. The crossover from inverted to normal structure occurs when $E_{s_c} = -1.39$ eV. The parameters were chosen so that the valence-band edge of each constituent is the same and defines the zero of energy.

For the first model alloy E_{s_c} was chosen to be 0.65 eV for one component and 0.5275 eV for the other. The first choice gives a compound semiconductor with the same band gap, 1.558 eV, as CdTe, while the second choice gives a compound which is almost CdTe with a band gap of 1.466 eV. The band structure of the two compounds is shown in Fig. 1. The differences are not noticeable on the scale of the figure.

Attempts were originally made to model the second alloy using $E_{s_c} = -1.8$ eV for the HgTe-like component and $E_{s_c} = 0.65$ eV for the CdTe-like component. Although the resulting band gaps were correct for HgTe and CdTe, the alloy effects of the mixture were too large. In fact, the conduction band separated into HgTe and CdTe bands. This separation does not happen in real $Hg_{1-x}Cd_xTe$ alloys. Instead, another choice was made for the E_{s_c} that reduced the alloy effects by reducing the difference between the E_{s_c}. The use of $E_{s_c} = -1.6$ eV provides a com-

TABLE I. Tight-binding parameters (in eV) used in this work. Except for E_{s_c}, the same value of each parameter is used for every constituent compound semiconductor.

E_{p_c}	E_{p_a}	E_{s_a}	$E_{s_a^*}$	P_1	P_2	S_1	S_2	S^*
4.8107	0.9167	−9.0	10.5	1.05	2.0	2.0	2.25	1.5

TABLE II. The CPA and VCA alloy conduction-band edges and the VCA surface-state energies for cation and anion terminated chains as a function of the cation s energy levels and x, the concentration of cation 2.

E_{s_c} (eV)			Conduction-band edge (eV)		VCA surface state (eV)	
Cation 1	Cation 2	x	VCA	CPA	Cation	Anion
0.5275	0.65	0.0	1.466	1.466	1.381	0.562
0.5275	0.65	0.2	1.483	1.474	1.400	0.565
0.5275	0.65	0.5	1.513	1.495	1.429	0.569
0.5275	0.65	0.8	1.541	1.523	1.456	0.573
0.5275	0.65	1.0	1.558	1.558	1.475	0.576
−1.6	−0.3063	0.2	0.04		0.035	
−1.6	−0.3063	0.5	0.33	0.13	0.30	0.26
−1.6	−0.3063	0.8	0.63	0.33	0.57	0.38
−1.6	−0.3063	1.0	0.83	0.83	0.76	0.44

pound with an inverted structure, while use of $E_{s_c} = -0.3063$ eV provides a direct-gap semiconductor with a gap of 0.83 eV. The cation levels were chosen so that the band gap occurs in the alloy first for $x \approx 0.2$ as in real $Hg_{1-x}Cd_xTe$. The inverted band structure for $E_{s_c} = -1.6$ eV is shown in Fig. 1.

The conduction-band edges predicted by the CPA and by the VCA, and the VCA alloy surface-state energies for cation and anion terminated chains are listed in Table II. Results are presented for the constituent compounds and for alloys with a 50-50 mixture and a 20-80 mixture. The band edges predicted by the VCA and by the CPA differ by less than 0.02 eV when the constituents are similar. The surface-state energies of like constituents are also similar. The surface state on a cation terminated chain shifts by 0.094 eV as x changes from 0.0 to 1.0. The surface state on the anion terminated chain shifts only 0.014 eV because the state is anion derived. In contrast, the CPA predicts substantial additional band-gap narrowing for the $Hg_{1-x}Cd_xTe$ alloy. In this case the surface states exist when $x = 1.0$, but not when the gap closes. Moreover, the VCA surface state of the anion terminated chain moves out of the gap when $x = 0.2$ even though the band gap is still finite in the VCA.

Figures 2–10 present the results for the surface DOS of cation and anion terminated chains. In every case the surface DOS is taken to be the contribution from all states on the cation and anion pair closest to the chain end. In practice, the major contribution to the surface DOS is made by the atom on the surface site. The DOS is determined by evaluating the Green's function at energies with a small imaginary part (0.001 eV), which broadens the DOS. The imaginary part is chosen small so that it does not add appreciably to the alloy broadening or qualitatively change the structure in the DOS. Small changes in this imaginary part do change peak heights in the DOS. The same imaginary part is used for each DOS so that comparisons of different DOS will be meaningful.

Figures 2–4 show the surface DOS near the conduction-band edge of a cation terminated chain when the alloy is a mixture of CdTe and "almost" CdTe. Arrows at the top of each figure indicate the locations of surface states (SS) and conduction-band edges (CB) for CdTe (cation 2) and almost CdTe (cation 1). The concentration of CdTe is given by x. The solid curve in each figure is the cluster calculation found using a CPA bulk and six cation-anion pairs in the cluster. The short-dashed curve is the CPA calculation which treats the four cations closest to the surface differently from the bulk. The long-dashed curve gives the VCA conduction band and the location of the VCA surface state.

The surface DOS of a cation terminated chain is atomic in character in the gap. The DOS has a bimodal distribution with the peaks occurring close to the surface-state energies of the constituents. The dominant peak of the pair

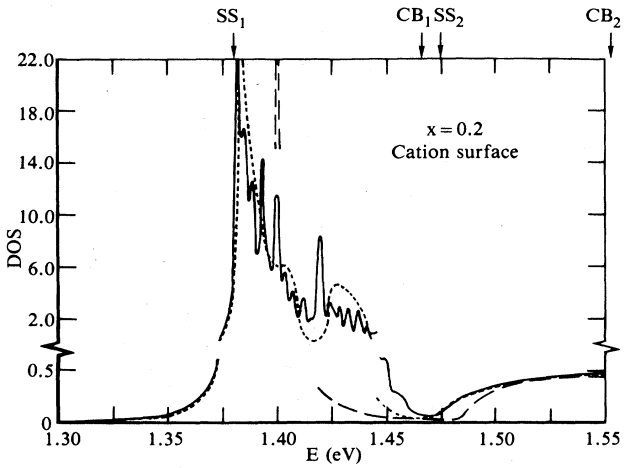

FIG. 2. Surface density of states of a cation terminated chain. $E_{s_c} = 0.5275$ and 0.65 eV for cations 1 and 2. Each constituent has a normal band structure. The concentration of cation 2 is $x = 0.2$. The solid curve is the cluster calculation using six cations in the cluster and a CPA bulk. The long-dashed curve indicates the VCA conduction-band edge and the location of the VCA surface state. The short-dashed curve shows the CPA calculation using four cations in the surface region. The surface states (SS) and conduction-band edges (CB) of the constituents are indicated by arrows.

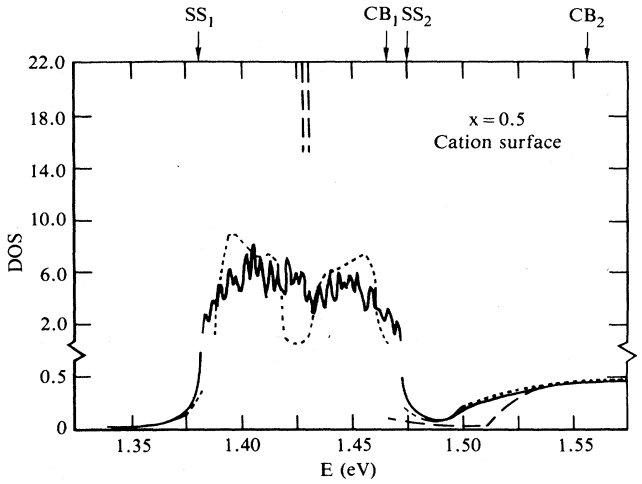

FIG. 3. Surface density of states of a cation terminated chain for $x = 0.5$. The constituents and curves are the same as in Fig. 2.

is associated with the surface state of the predominant cation in the alloy. The CPA and the cluster calculations predict qualitatively similar DOS, both with bimodal distributions and with similar variations as a function of composition. The CPA also correctly predicts the structure of each peak that is correlated to the occupancy of the cation next to the surface cation. The width of the CPA surface-state band is slightly narrower than that predicted by the cluster calculation. However, both calculations predict the same band edge for the dominant peak. The states in the surface-state band are well localized to the chain end because the cluster calculations do not change significantly when the cluster size is increased or a VCA bulk is used rather than a CPA bulk. The VCA predicts a single discrete surface state, whose broadening is determined by the choice of the imaginary energy used to evaluate the Green's function. The VCA surface state lies between the peaks in the bimodal structure. However,

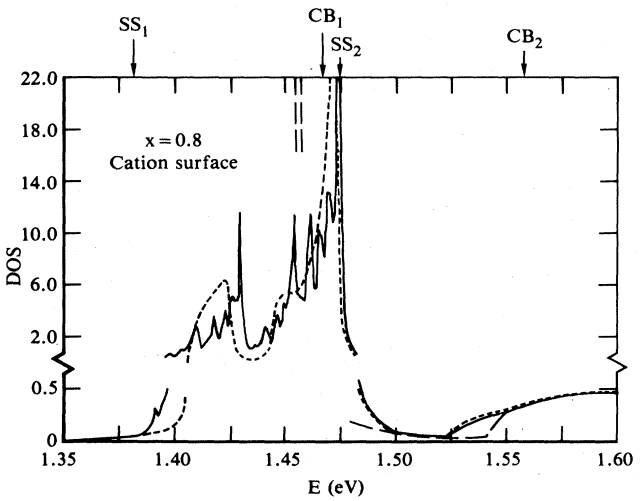

FIG. 4. Surface density of states of a cation terminated chain for $x = 0.8$. The constituents and curves are the same as in Fig. 2.

no feature in the cluster surface DOS is reproduced by the VCA.

The surface DOS of anion terminated chains are not shown, but they also exhibit a bimodal distribution with peaks near the constituent surface-state energies and peak heights correlated to the alloy composition. The width of the anion surface-state band is an order of magnitude smaller than the width of the cation surface-state band, because the anion surface-state energies of the constituents differ by only 0.014 eV. The CPA and cluster DOS are again nearly identical with the cluster DOS being slightly broader. The appearance of the bimodal distribution for the anion terminated chain was unexpected since the anion-derived valence bands are insensitive to the alloy fluctuations. This distribution indicates that alloy effects are more severe for localized states than for extended states.

The surface states of the cation terminated chain are derived from the cation s level with a weak admixture of those anion levels which couple to the cation s level. At the peak in the surface DOS the states are 80% cation s,

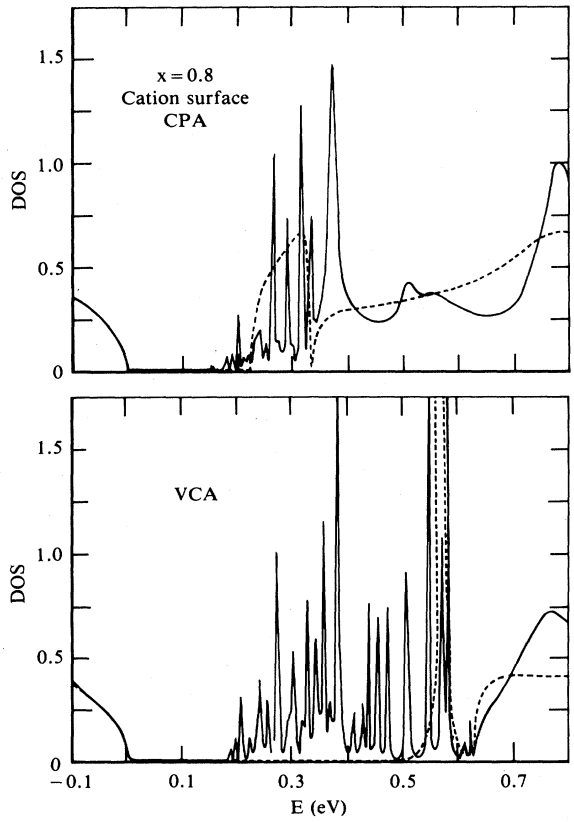

FIG. 5. Surface density of states of a cation terminated chain. Cation 1 has an inverted band structure and $E_{s_c} = -1.6$ eV. Cation 2 has the normal band structure, $E_{s_c} = -0.3063$ eV, and concentration $x = 0.8$. The solid curves show the cluster calculations using six cations in the cluster and a CPA or VCA bulk (in the respective halves of the figure). The dashed curves are the CPA calculation with four surface cations and the VCA calculation in the respective halves.

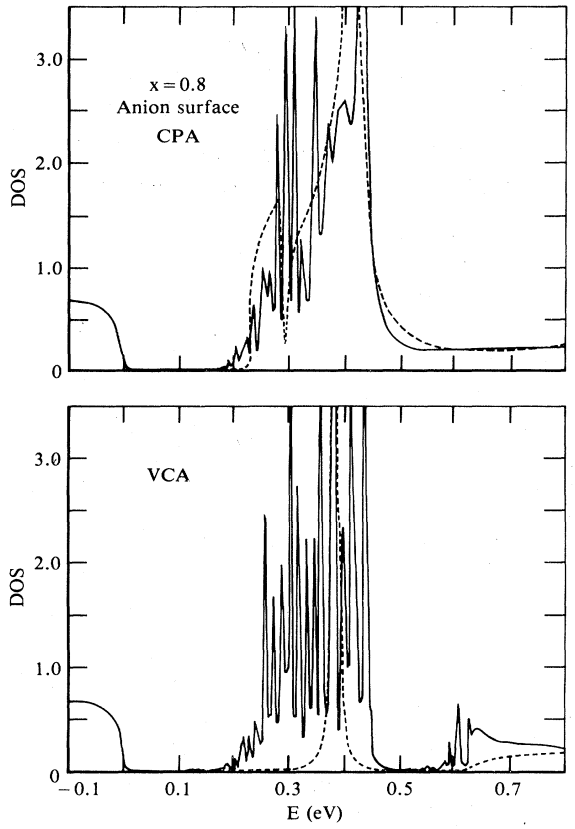

FIG. 6. Surface density of states for an anion terminated chain with $x = 0.8$. The constituents and curves are the same as in Fig. 5.

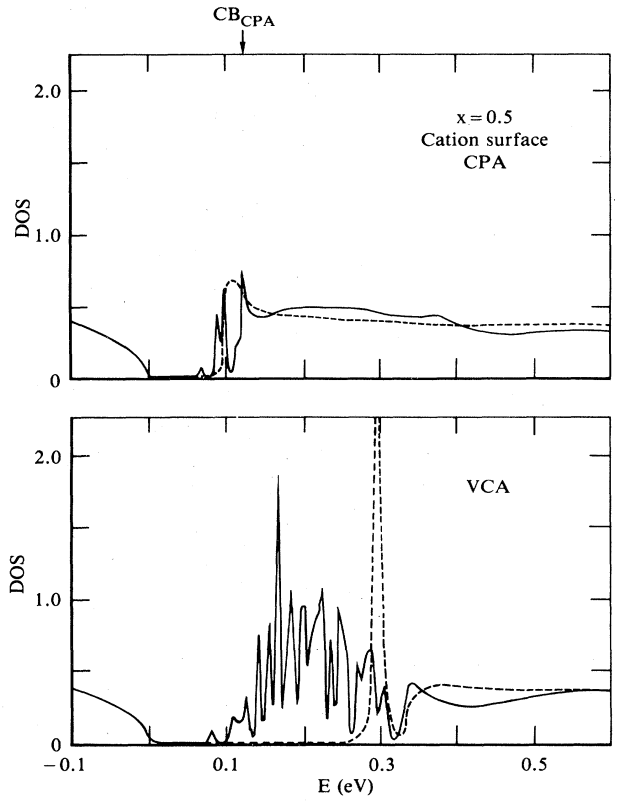

FIG. 7. Surface density of states for a cation terminated chain with $x = 0.5$. The constituents and curves are the same as in Fig. 5. CB_{CPA} indicates the CPA conduction-band edge.

10% anion s, 6% anion s^*, and 4% anion $p_{3/2}$. The surface states of the anion terminated chain are derived primarily from the anion $p_{1/2}$ state (62%), which produces the heavy-hole band and is the most easily localized level, the anion $p_{3/2}$ state (24%), the cation s level (6%), and the cation $p_{1/2}$ level (4%). These percentages do not change much for different alloy compositions.

The surface DOS of the $Hg_{1-x}Cd_xTe$-like alloy are shown in Figs. 5—10. Results for cation and anion terminated surfaces and for $x = 0.2$, 0.5, and 0.8 are included (x is the concentration of the CdTe-like constituent). The results for the anion terminated chains are shown because the alloy effects on such chains are much greater for HgCdTe-like alloys than they were for the first alloy considered. The alloy effects in HgCdTe-like alloys are larger because the anion derived bands can be either normal or inverted depending on the cation environment in the HgCdTe alloys. The alloy effects are sufficiently strong in the HgCdTe alloys to induce a large CPA band-gap bowing (see Table II). Because the CPA and the VCA conduction bands differ by so much, cluster calculations have been done using both the CPA and the VCA for the bulk. In contrast, the VCA, CPA, and cluster valence bands are nearly identical near the band gap. As a result, only the cluster valence band is shown when $x = 0.5$ and 0.8.

The CPA and VCA cluster calculations are very similar especially when $x = 0.5$ and 0.8. Both show states below the CPA conduction-band edge with comparable structure and onsets. Above the CPA band edge the CPA cluster calculation predicts a continuous DOS with structure resulting from surface resonances. The VCA cluster calculation has distinct peaks below the VCA band edge. However, when these peaks are smoothed, the resulting structure can be identified with structure in the CPA cluster calculation. When $x = 0.2$, the CPA band gap is closed. In the analogous VCA cluster calculations, additional states appear below the VCA band edge, substantially reducing the gap but not completely closing it. The similarity of the two cluster calculations, especially between the CPA and VCA band edges where the VCA calculation predicts only discrete localized states, indicates that the CPA should provide a better description of the bulk conduction-band states and their effect on the surface DOS for this model alloy.

HgTe-like chains have no band gap and thus no surface states. However, pure CdTe chains do have surface states. These states lie above the CPA band edges for $x \leq 0.8$. The cluster calculations of localized states are sensitive to the local environment near the surface and reflect the atomic character of the end of the chain. Thus the resonance structure observed above the band gap in Figs. 5—8

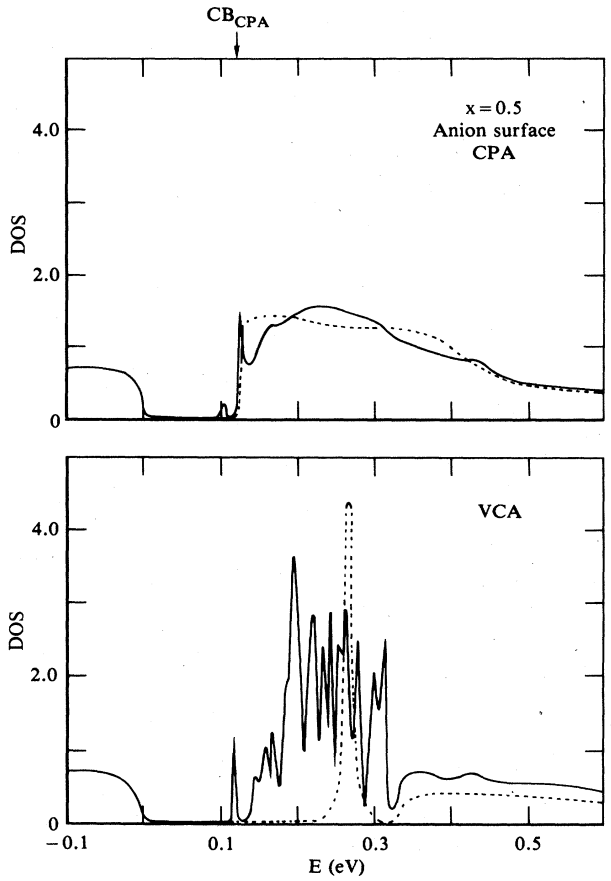

FIG. 8. Surface density of states for an anion terminated chain with $x=0.5$. The constituents and curves are the same as in Fig. 5.

can be interpreted as CdTe surface states resonant with the CPA conduction band.

One would expect the VCA to predict discrete surface states located at average energies which depend on x. The VCA surface DOS does have narrow surface-state peaks below the conduction-band edge when $x=0.5$ and 0.8.

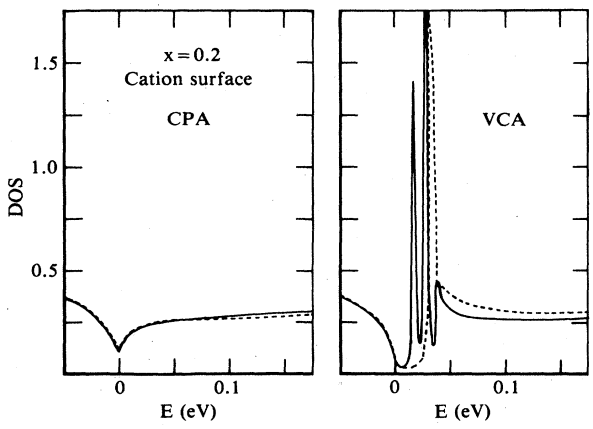

FIG. 9. Surface density of states for a cation terminated chain with $x=0.2$. The constituents and curves are the same as in Fig. 5.

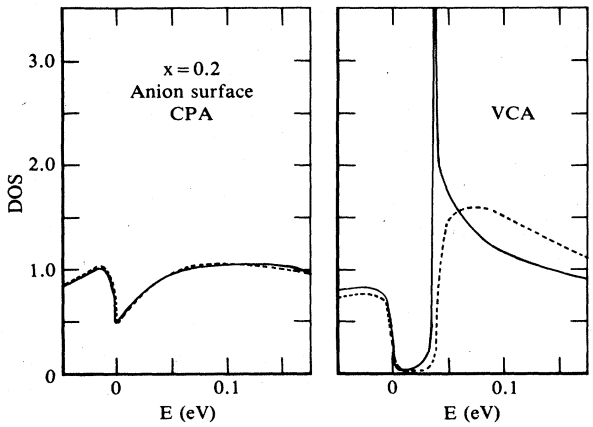

FIG. 10. Surface density of states for an anion terminated chain with $x=0.2$. The constituents and curves are the same as in Fig. 5.

When $x=0.2$, this peak occurs just below the conduction-band edge for a cation terminated chain and has moved out of the gap for an anion terminated chain. These VCA surface states occur well above the CPA band edge in each case and cannot be consistently identified with any sharp structure in the CPA or VCA cluster calculations.

On the other hand, the CPA calculations, with four cations in the surface region, are qualitatively similar to the two cluster calculations. The CPA predicts surface states in the band gap near the band edge as predicted by the cluster calculations. The shape of the CPA surface DOS is similar to a smoothed cluster surface DOS, especially when $x=0.8$, except that the CPA band tailing extends slightly less into the gap. This difference in width also occurred for the surface-state bands of the first alloy considered. The CPA is unable to reproduce the detail of the resonance structure above the band edge. However, when the resonance structure is smoothed, the qualitative agreement between the CPA and the cluster calculations is good. This observation, that the CPA more reliably predicts the details of the surface DOS for localized levels than for extended resonance states, was also true in our previous calculations.[1] When $x=0.2$ and the CPA gap vanishes, no surface states exist. In this case the CPA cluster calculation and the CPA calculation agree almost exactly.

The surface states of the HgCdTe alloys are similar in makeup to those for alloys made from normal semiconductors. The surface states of a cation terminated chain are derived from cation s levels and the anion states, primarily $p_{3/2}$ and s, that couple to it. For $x=0.8$ the percentages are 63, 28, and 9, respectively; and for $x=0.5$ they are 69, 17, and 14, respectively. The surface states of anion terminated chains are derived from anion $p_{1/2}$ states (67%) and cation s (20%) and $p_{1/2}$ (13%) states.

In our previous work[1] reliable results were obtained when the CPA calculations were done with three or four cations in the surface region. Our present calculations

show that using three or four cations is still sufficient for more realistic models. For example, when the surface DOS of an alloy made from two normal constituents with $x=0.8$ (see Fig. 4) is calculated using only one surface cation, two sharp peaks occur in the DOS near 1.42 and 1.465 eV. When two surface cations are used, the lower peak shifts to slightly higher energy and a low-energy shoulder appears. The upper peak also shifts to higher energy and a third peak appears at 1.45 eV. As the number of cations used increases, this third peak broadens into the plateau seen in Fig. 4 and the other two sharp peaks broaden. When more than four surface cations are used, the peaks and the total width of the surface band broaden slightly, but the improvement in the DOS does not merit the extra effort used to obtain it.

IV. SUMMARY AND CONCLUSIONS

We have assessed the effects of alloy fluctuations on the surface states of ternary semiconductor alloys by performing embedded-cluster calculations. The ability of the VCA and multisurface CPA to incorporate these alloy effects has also been tested. The calculations were performed for model one-dimensional semi-infinite chains of alternating anion and randomly occupied cation sites, each atom described by a set of realistic levels. The model is simple but it allows one to gain the insight needed to model real systems.

Despite the inherent alloy broadening, the surface DOS of the one-dimensional alloys considered here retain much of the atomic character of the surface DOS of their individual constituents. This is similar to the narrowing of the surface DOS manifested by previous work. The results show that the surface states are sensitive to the local environment near the surface even when the alloy effects on the extended states are small.

As a result of the diagonal disorder, the alloy made from two similar normal semiconductors has a bimodal surface DOS, with the peaks correlated to the surface states of the alloy constituents. The bimodal distribution occurs not only for the cation terminated chain, where the surface site is a randomly occupied cation site, but also for anion terminated chains where the randomly occupied site is the neighbor of the surface site. The CPA provides a reliable approximation for the DOS. It correctly reproduces the shape and width of the bimodal distribution for both cation and anion chains. The VCA predicts a narrow surface-state peak located at an average energy of the bimodal distribution. Similar bimodal distributions occur for the DOS of the more localized deep valence-band states in $Hg_{1-x}Cd_xTe$.[19,20] Cluster calculations[12,13] of alloy broadening of impurity levels also show DOS which are sensitive to the local environment.

The surface states of the CdTe-like constituent of a HgCdTe-like alloy occur well above the CPA band edge for most alloy compositions, while the HgTe constituent has no surface states. Because the alloy surface states are sensitive to the local environment, the alloy surface DOS has resonance structure above the CPA band edge, substantial band tailing below the edge, but no surface-state band that is well separated from the bulk states. The alloy effects are substantial for anion terminated chains as well as cation terminated chains even though the valence band of extended states is unaffected by the alloy fluctuations. This observation is further evidence of the sensitivity of the surface states to the local environment and thus to alloy fluctuations.

The VCA predicts a narrow surface-state peak which is not correlated to any structure in the cluster DOS. In contrast the CPA incorporates the effects of fluctuations in the local environment and reproduces the band tailing of surface states into the gap. The CPA works equally well for both chain terminations. The similarity of the cluster calculations done using either the CPA or the VCA for the bulk, especially in the region below the VCA band edge, indicates that the CPA also gives a much better description of the conduction band for this model alloy.

In practice, only the four cations nearest the surface need to be treated differently from the bulk cation to obtain the information available in a multisurface CPA calculation. The use of more sites only broadens the alloy DOS slightly.

Only diagonal disorder in the cation s level has been included in our model. When off-diagonal disorder is included, the resulting disorder in the hopping terms of the Hamiltonian should directly affect the widths of the DOS. In addition, the strength of the hopping determines how localized a surface state is to the surface. Thus the sensitivity of the surface state to alloy fluctuations near the surface, which depends on this localization, should also be affected by hopping disorder.

Systems with anion disorder have not been considered. However, several comments can be made about the possible effects of anion disorder. Our results indicate that for normal semiconductors the states localized to a cation surface are predominantly cation s states, while there is substantial mixing of anion p levels in states localized to anion surfaces. Thus the surface states at anion surfaces of alloys with anion disorder may be more sensitive to off-diagonal disorder than other surface states are. In addition, the states localized to an anion surface are derived from valence-band states. These band states have larger effective masses than the conduction-band states have and should be more localized. Thus states localized to anion surfaces of alloys with anion disorder may be more sensitive to local fluctuations in site occupation than are states localized to cation surfaces of alloys with cation disorder. The magnitude of the anion disorder effects on the surface states will depend on the scale of the anion p level disorder. Detailed calculations for alloys with anion disorder should be carried out before quantitative statements about the relative importance of cation and anion disorder are made.

The calculations have been performed for one-dimensional-model systems so that the Green's functions could be obtained simply and the cluster averages done easily. However, there are limitations to one-dimensional models which should be kept in mind when extrapolating to three-dimensional systems. As discussed in the Introduction, the sensitivity of the surface DOS to the local environment is determined, in part, by the number of sites that the localized surface states sample. In three-

dimensional systems the states sample more sites so the alloy effects should be less severe, the states will be less sensitive to the local environment, and there will be less alloy broadening.

The surface of a three-dimensional system can be constructed by coupling together an array of chains, all extending perpendicular from the surface. For a normal semiconductor the coupling between chains broadens the surface state of a single chain into a surface-state band. For an alloy, the coupling between chains will broaden the individual peaks of the bimodal surface DOS of a single chain into bands. The actual shape of the DOS will depend on the energy separation between peaks, the extent of the banding, and the amount of alloy broadening. When the alloy is a mixture of constituents which have surface states that are well separated in energy and have little dispersion across the surface Brillouin zone, the surface DOS of the alloy should be bimodal. When the constituents have surface states which are close in energy and vary substantially in energy across the surface Brillouin zone, the bimodal character of the DOS will be lost.

Our calculations have shown that the atomic character of the surface DOS is maintained when a one-dimensional alloy is formed by mixing its constituents, despite the inherent alloy broadening. The banding which occurs when the system becomes three dimensional may or may not destroy this atomic character of the surface DOS. Whether this occurs for a particular three-dimensional system will depend on the details of the system and must be determined by specific calculations for that system.

ACKNOWLEDGMENTS

This work was performed under the McDonnell Douglas Independent Research and Development program.

[1]G. W. Bryant, Surf. Sci. (to be published).
[2]N. F. Berk, Surf. Sci. **48**, 289 (1975).
[3]M. C. Desjonqueres and F. Cyrot-Lackman, J. Phys. F **7**, 61 (1977).
[4]A. Gonis and J. W. Garland, Phys. Rev. B **16**, 2424 (1977).
[5]A. Gonis, W. H. Butler, and G. M. Stocks, Phys. Rev. Lett. **50**, 1482 (1983).
[6]A. Gonis, G. M. Stocks, W. H. Butler, and H. Winter, Phys. Rev. B **29**, 555 (1984).
[7]A. Gonis and A. J. Freeman, Phys. Rev. B **29**, 4277 (1984).
[8]C. W. Myles and J. D. Dow, Phys. Rev. Lett. **42**, 254 (1979).
[9]C. W. Myles and J. D. Dow, Phys. Rev. B **19**, 4939 (1979).
[10]M. J. O'Hara, C. W. Myles, J. D. Dow, and R. D. Painter, J. Phys. Chem. Solids **42**, 1043 (1981).
[11]C. W. Myles, Phys. Rev. B **28**, 4519 (1983).
[12]C. W. Myles, J. D. Dow, and O. F. Sankey, Phys. Rev. B **24**, 1137 (1981).
[13]C. W. Myles and J. D. Dow, Phys. Rev. B **25**, 3593 (1982).
[14]P. Soven, Phys. Rev. **156**, 809 (1967).
[15]R. J. Elliot, J. A. Krumhansl, and P. L. Leath, Rev. Mod. Phys. **46**, 465 (1974).
[16]A.-B. Chen and A. Sher, Phys. Rev. B **17**, 4726 (1978).
[17]A.-B. Chen and A. Sher, Phys. Rev. B **23**, 5360 (1981).
[18]A.-B. Chen and A. Sher, J. Vac. Sci. Technol. **21**, 138 (1982).
[19]W. E. Spicer, J. A. Silberman, J. Morgan, I. Lindau, J. A. Wilson, A.-B. Chen, and A. Sher, Phys. Rev. Lett. **49**, 948 (1982).
[20]K. C. Hass, H. Ehrenreich, and B. Velický, Phys. Rev. B **27**, 1088 (1983).
[21]H. Ueba and S. Ichimura, Phys. Status Solidi B **92**, 307 (1979).
[22]A. Zagorski and W. Nazarewicz, Acta Phys. Pol. **A57**, 403 (1980).
[23]B. Velický and J. Kudrnovský, Surf. Sci. **64**, 411 (1977).
[24]I. Ishida, N. Inoue, and T. Matsubara, Prog. Theor. Phys. **55**, 653 (1976).
[25]See R. E. Allen and J. D. Dow, J. Vac. Sci. Technol. **19**, 383 (1981), for a list of references.
[26]R. E. Allen, H. P. Hjalmarson, and J. D. Dow, Surf. Sci. **10**, L625 (1981).
[27]R. E. Allen and J. D. Dow, Phys. Rev. B **25**, 1423 (1982).
[28]A. C. Redfield, M. A. Bowen, K. E. Newman, and J. D. Dow, Solid State Commun. **46**, 371 (1983).
[29]J. Singh and A. Madhukar, Phys. Rev. B **25**, 7700 (1982).
[30]C. A. Swarts, M. S. Daw, and T. C. McGill, J. Vac. Sci. Technol. **21**, 198 (1982).
[31]A. Kobayashi, O. F. Sankey, and J. D. Dow, Phys. Rev. B **25**, 6367 (1982).
[32]P. Vogl, H. P. Hjalmarson, and J. D. Dow, J. Phys. Chem. Solids **44**, 365 (1983).
[33]H. P. Hjalmarson, P. Vogl, D. J. Wolford, and J. D. Dow, Phys. Rev. Lett. **44**, 810 (1980).
[34]H. Aoki, J. Phys. C **13**, 3369 (1980).
[35]C. E. T. Goncalves da Silva and B. Koiller, Solid State Commun. **40**, 215 (1981).
[36]B. Koiller, M. O. Robbins, M. A. Davidovich, and C. E. T. Goncalves da Silva, Solid State Commun. **45**, 955 (1983).
[37]A.-B. Chen, Phys. Rev. B **7**, 2230 (1973).